LA-UR-17-28844
Approved for public release; distribution is unlimited.

Title: HFIR Fuel Casting Support

Author(s): Imhoff, Seth D.
Gibbs, Paul Jacob
Solis, Eunice Martinez

Intended for: Report

Issued: 2017-09-28

HFIR Fuel Casting Support

Seth Imhoff[1,*], Paul Gibbs[1], Eunice Solis[1]

[1]Sigma Division, Los Alamos National Laboratory,
M.S. G770, P.O. Box 1663, Los Alamos, NM 87545
*Corresponding Author, sdi@lanl.gov

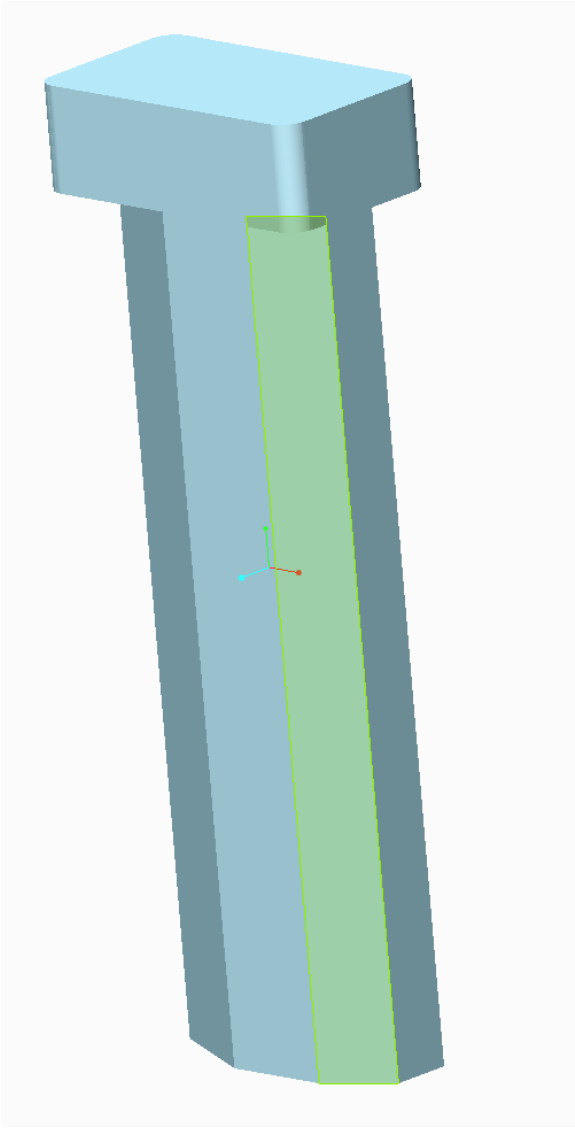

HFIR Fuel Casting Support

Seth Imhoff[1,*], Paul Gibbs[1], Eunice Solis[1]

[1]Sigma Division, Los Alamos National Laboratory,
M.S. G770, P.O. Box 1663, Los Alamos, NM 87545
*Corresponding Author, sdi@lanl.gov

Summary

Process exploration for fuel production for the High Flux Isotope Reactor (HFIR) using cast LEU-10wt.%Mo as an initial processing step has just begun. This project represents the first trials concerned with casting design and quality. The studies carried out over the course of this year and information contained in this report address the initial mold development to be used as a starting point for future operations. In broad terms, the final billet design is that of a solid rolling blank with an irregular octagonal cross section. The work covered here is a comprehensive view of the initial attempts to produce a sound casting. This report covers the efforts to simulate, predict, cast, inspect, and revise the initial mold design.

1.0 Design Definition

In order to prepare for future production of a monolithic U-10wt.%Mo fuel for HFIR, a unique set of challenges are presented by the overall fuel shape. Potential paths forward were provided by LANL during FY15 with some limited funding in FY16. However, the design definitions were not forthcoming until June of 2016 so only a small amount of work was performed in that year.

Once guidance was provided, a new work task plan took these considerations into account and work began to produce the desired castings. Starting from the expected inner fuel element details which are shown schematically in Figure 1, the fuel designers determined the bounding limits of the final cast shape.[1]

The resultant starting shape was determined to be a solid billet with an irregular octagonal cross section. The acceptable final rolling billet was determined to be between 9 inches and 5 inches long. Ignoring the tapered ends for the moment, the overall width was determined to be 1.44 inches (minor axis) and the height to be 3.07 inches (major axis). Details of this final rolling billet shape are given in Figure 2.

It was prescribed that the overall design should be compatible with other VIM furnace designs and the hot top[1] should be no more than 15% of the total casting mass. In any manufacturing environment, the total product yield should be maximized.[2]

[1] The “hot top” as used here is a portion of the casting which has a longer solidification time and acts to feed liquid metal to areas which would otherwise form voids due to shrinkage during solidification. For uranium VIM casting this is generally located at the top of the casting. Other related terms are “riser” or “lug.”
[2] Total product yield is the final cast product mass divided by the initial charge mass.

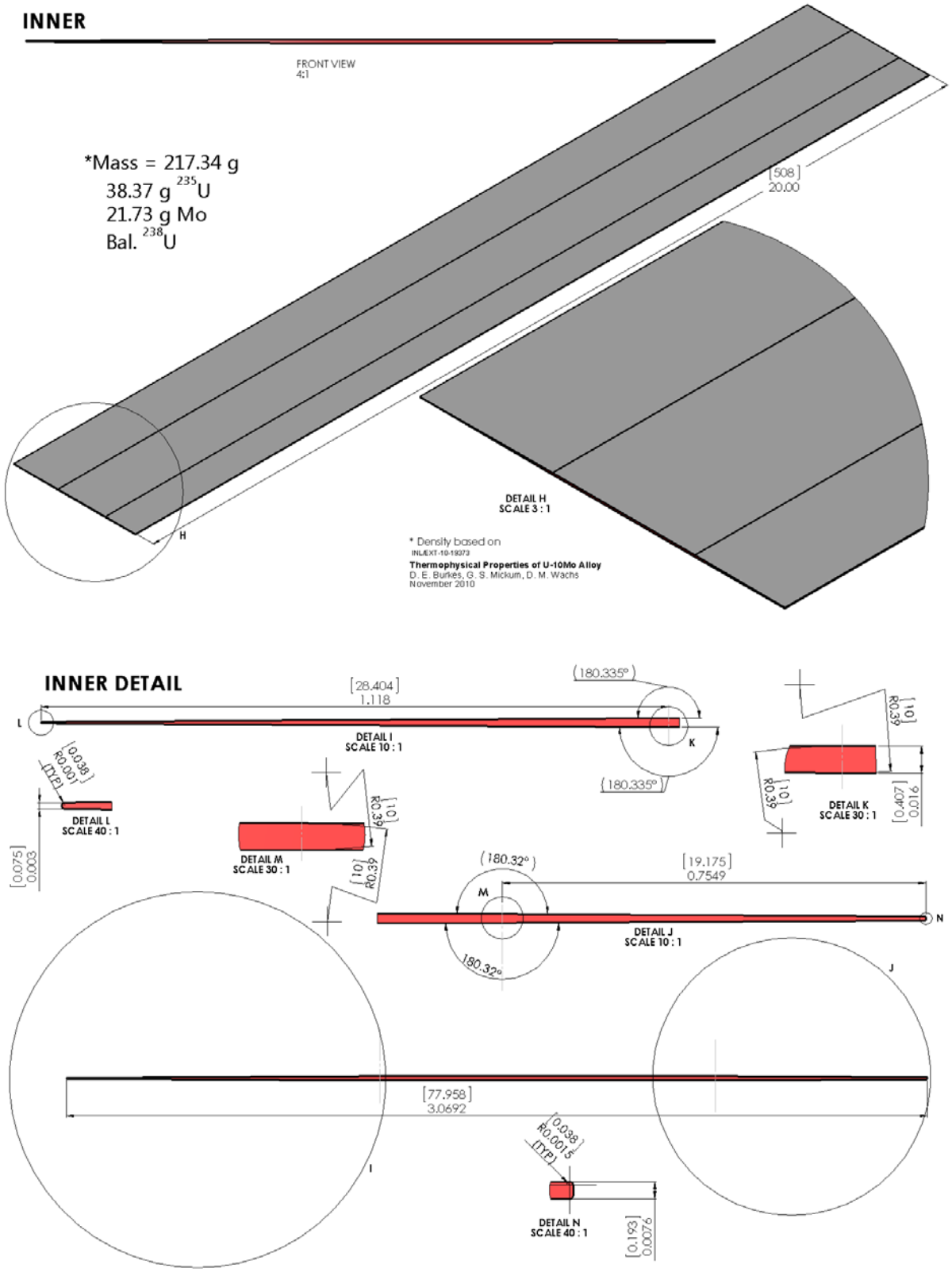

Figure 1: Schematic drawing of a HFIR inner fuel element from the interim fuel design [1].

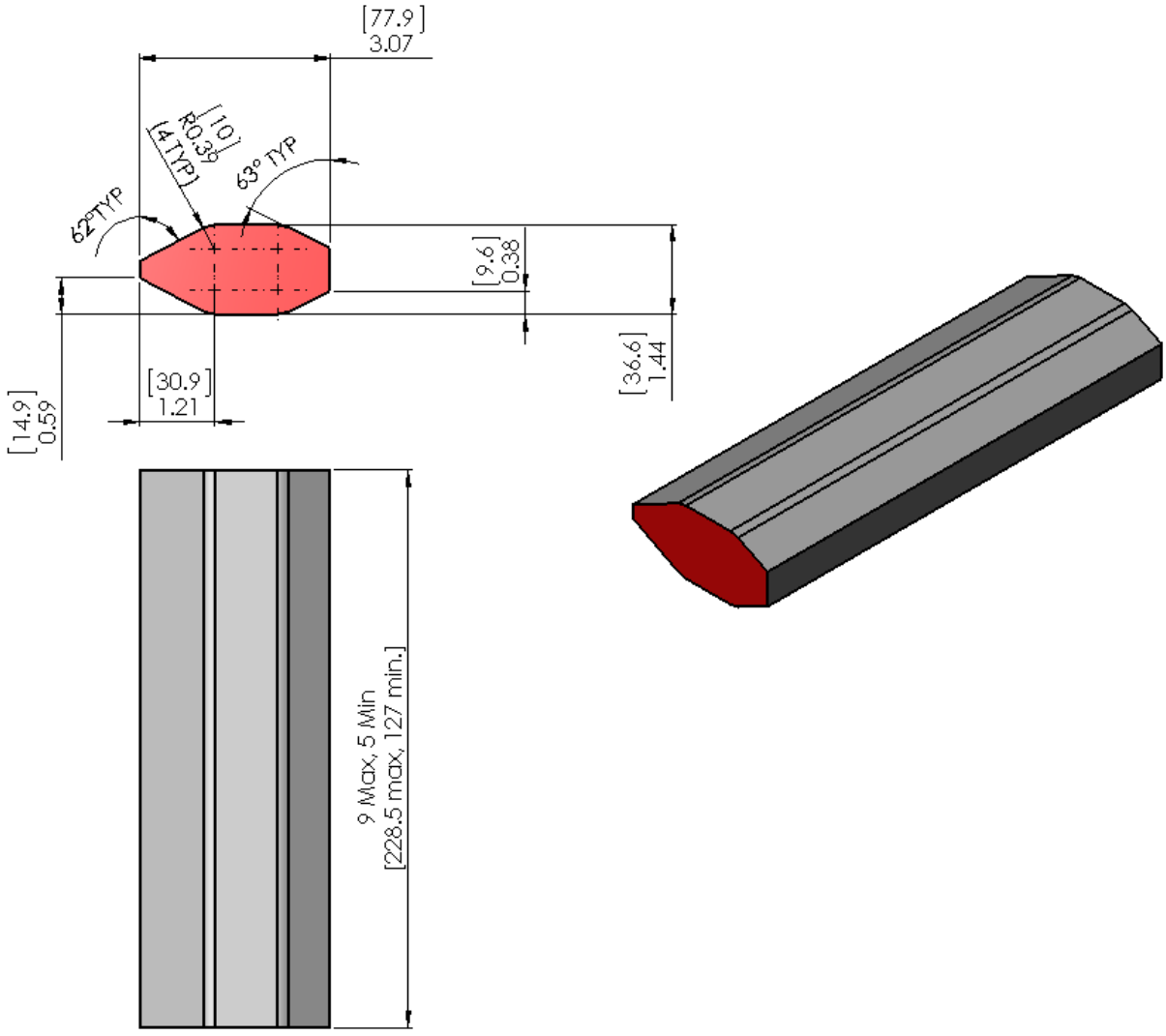

Figure 2: Finished rolling billet suitable for production of a HFIR inner fuel foil. [1]

While the priorities for mold design are listed explicitly in the following section, the general landscape of part design and mold design should be explained. For any given component, there are a variety of engineering properties which are determined by the designers. One straight forward example would be with strength. A figure is given below which corresponds well with the concept of strength as one of these important properties.

The final assembly of component parts will impose a set of geometric constraints. These geometric constraints can be considered arbitrary and assume any range of property values so long as they fit the design dimensions. Generally, this means that the corresponding part can be of a small size so long as it fills the property need. However, there is a property-driven constraint which corresponds to a minimum set of values. For instance, a minimum strength requirement may be set. Within the adjustable parameter space (for both design and processing), this sets the options which may be explored. Real materials with real geometric constraints would then occupy the space in Figure 3 outside of the red area, but within the gray area. Once a material class is selected, this is further downsized by the achievable properties.

The final properties of any material class may be broadly driven by two types of features. The first is related to defects. For strength this could mean large inclusions or voids. For something more relevant to this project, it could mean neutron absorption properties in the form of chemical macrosegregation.

At a finer scale, the second set of features becomes more prevalent and is related to optimum performance of a material class. That is the microstructure of the final part. For strength this could relate to the final grain size or even the phases that are present within the material. This same concept could be applied to neutron absorption, by imagining that microsegregation would change local behavior.

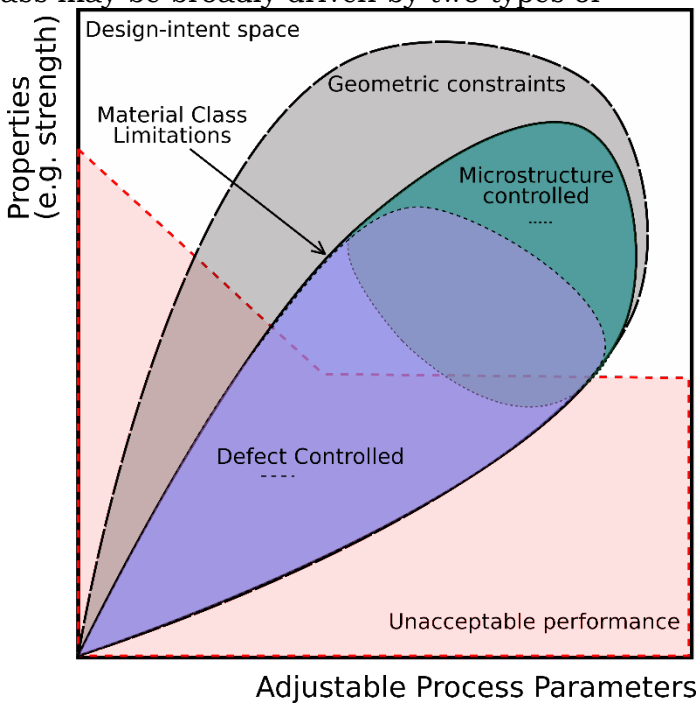

Figure 3: A schematic diagram showing the types of design concerns when addressing final properties and adjustable parameters.

This project is wholly concerned with the macro properties and achieving a sound casting. Some baseline information may be available concerning the microstructural effects, but until further development is achieved, there will be no strong linkages to final properties (within the broad range of material class) other than that found in other sources.

2.0 Initial Design Considerations

The initial design was based upon the following prioritized list of parameters

1. Maximize the length of the final rolling billet (9 in).
2. Maximize the thermal gradient while minimizing cold laps.[3]
3. Minimize the hot top size.
4. Utilize design features that are transferrable to other manufacturing sites.
5. Determine the cross section dimensional stability.

In order to maximize the overall length of the rolling billet, the design guidance maximum was taken as the goal length. Since gap formation at the bottom of the casting was anticipated and some shrinkage occurs, the total length must be extended if the final length is to be as close as possible to 9 in. Additionally, our standard method of hot top removal involves a bandsaw cut with a kerf[4] of approximately 0.125 in. Therefore, the total length of the mold with the designed cross section was set to 9.25 in to accommodate these accumulated losses in length.

The thermal gradient was maximized by incorporating a relatively thin mold wall with large mold clamps on the top and bottom to act as a heat source and sink respectively. The mold stack assembly was placed in the furnace so that the upper half of the stack, that includes the crucible, top clamp, and upper mold was well within the induction coils while the bottom half of the mold would rely more heavily on conduction for heating. It should be noted that placement of the mold stack relative to the induction coils is a critical parameter and will be discussed further in the following section on simulation results.

The mold design left considerable margin for a decision on overall hot top height. The cavity height for the hot top is 1.75 inches. While the desired hot top is considerably shorter than this cavity height, one goal in mold design is to ensure that the molten metal in the hot top does not impinge upon an upper mold surface so as not to start freezing top-down. This goal is to prevent massive void formation within the part itself. Additionally, the extra cavity height provides a considerable amount of design and charging flexibility should it be necessary.

The ideal maximum hot top size can be determined from the relative areas of the cavities. The billet cross sectional area is 3.47 in^2 so the volume of the total billet is 32.08 in^3. The hot top cavity area is 6.95 in^2 so for the hot top to be a maximum of 15% of the total casting volume, the height necessary is 1.86 in or less.

In order for smooth technology transfer, the main consideration for this casting is the crucible design. A 10 in DIA crucible design was used in these casting trials. The only significant difference is the pouring mechanism. LANL uses a stopper rod design while other facilities use a knock-out assembly. To explain, a knock-out assembly utilizes a crucible with a thin layer of graphite covering the pour hole. At pour-time a rod is lowered and knocks out the graphite disk which is caught by a graphite cage to

[3] A cold lap can be defined as a surface void caused by quick-freezing of metal against the mold wall which is not backfilled by melt inflow. This usually occurs when a mold is too cold.
[4] Kerf is defined as the width of material removed during a cutting operation.

prevent it from entering the mold cavity while allowing the metal to flow through. Since this is not currently a pour-rod insert was used to adapt the crucible to this difference. Additionally, a small spacer disk was inserted between the crucible and the top mold clamp in order to represent potential heat flow differences that would occur if alternative splash guards or interfaces were utilized in a production environment. The mold interfaces are the critical part being anticipated, so the height was not determined to be as important at this time. Furthermore, if future work is necessary, this can be easily adapted for final comparison.

3.0 Simulation Results

3.1 Material parameters

It should be pointed out that while care is taken to use appropriate material parameters during simulation setup, these data should not be considered reference data. Reference data has been used where available, but this report does not discuss he overall accuracy of density (or other) measurements. Instead, insight is gained from the study with the advanced knowledge that some physical differences may be possible. Gross changes in material parameters will certainly create uncertainty in the accuracy of the predictions, but since real casting experiments were performed, this report does not rely upon these predictions to provide more than insight.

The parameters listed here are for the major components of graphite for the mold and DU-10Mo for the metal. Other material properties that are ancillary to the solution, such as the refractory brick, are given in the input files, but are not provided in this report.

3.1.1 Interfacial Heat Transfer Coefficient

One type of assumption for heat transfer is to distill interfacial properties down to a single coefficient. In many cases, this type of parameter does not need to be known with any high degree of precision so SME knowledge of reasonable constraints may be applied when data is unavailable. The most important heat transfer coefficients are between the metal and the mold wall as well as for mold-to-mold interfaces. Changes to the mold-mold interfacial heat transfer only become particularly necessary when pieces are not tight-fitting or when a high level of fidelity is absolutely necessary.

Interfacial heat transfer coefficients are difficult to measure directly and in certain cases must be re-measured for each mold design. For the current mold where there is a hot top, we can choose parameters which come from the Sigma Foundry and Solidification Science team's collective experience. Conceptually, this can be broken into three regimes as given in Table 1. When the molten metal is in contact with the mold, relatively intimate heat transfer is assumed. As the melt at the interface turns solid, an empirical gap model decreases the heat transfer by approximately 50%. Once the ingot is cooled more significantly (i.e. <800°C), the gap will have increased and a second decrease of 50% in heat transfer coefficient is assumed. A major gap will open once the hot top area has a solid shell, as it will lift the entire ingot off of the bottom surface. This condition is expected to be reasonably modeled with these assumptions.

Temperature Range [°C]	Heat Transfer Coefficient, h [W/(m²K)]	Comment
T ≥ 1175	2000	Melt contact
1175 > T > 800	1000	Gap formation
T ≤ 800	500	Significant gap

Table 1: Heat transfer coefficients used in the simulations with descriptions of the physical mechanisms that underpin those decisions.

3.1.2 Density

Graphite density [2] is based upon the coefficient of linear expansion, $a=4.5\times10^{-6}$ and the value at a reference temperature $T_R = 295\ K$. The equation is given below.

$$\rho_{Mold} = \frac{1.775}{1 + 3\alpha(T - T_R)}$$

The density for alloyed uranium is less well known. A survey of information as well as new data is available in a recent publication [3], but the complete behavior with temperature is not well characterized. Since this data cannot be considered strong reference data, some approximations for behavior have been used and a comparison with pure DU [4] is given in the figure below.

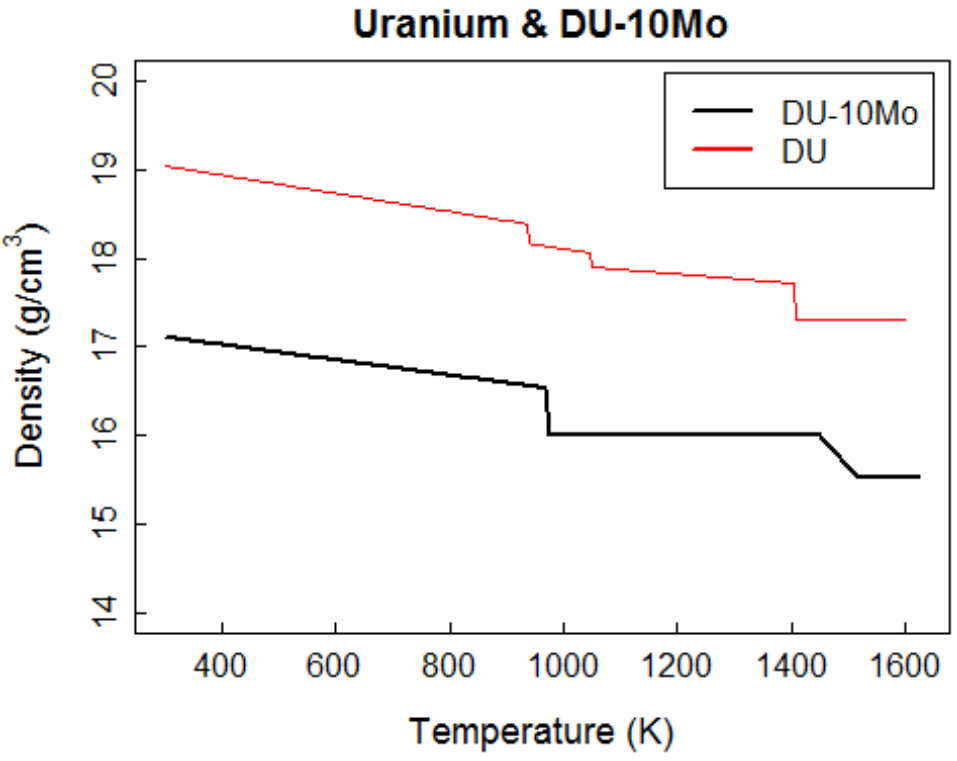

Figure 4: A comparison of density values for pure DU and the current estimate for DU-10Mo.

3.1.3 Thermal Conductivity

Data for the thermal conductivity of the metal comes from two references [3,4] (additional sub-references to be found in the literature). For DU-10Mo, raw data exists up to 800°C. For pure DU data exists from room temperature to beyond the melting point. Since pure DU does not appear to deviate in thermal conductivity from low temperature to high temperature, the data up to 800°C for the alloy was assumed to follow the same trend. Measured data does not exist for the liquid state of the alloy, so that of pure DU was used in its stead. A comparison can be seen in Figure 5.

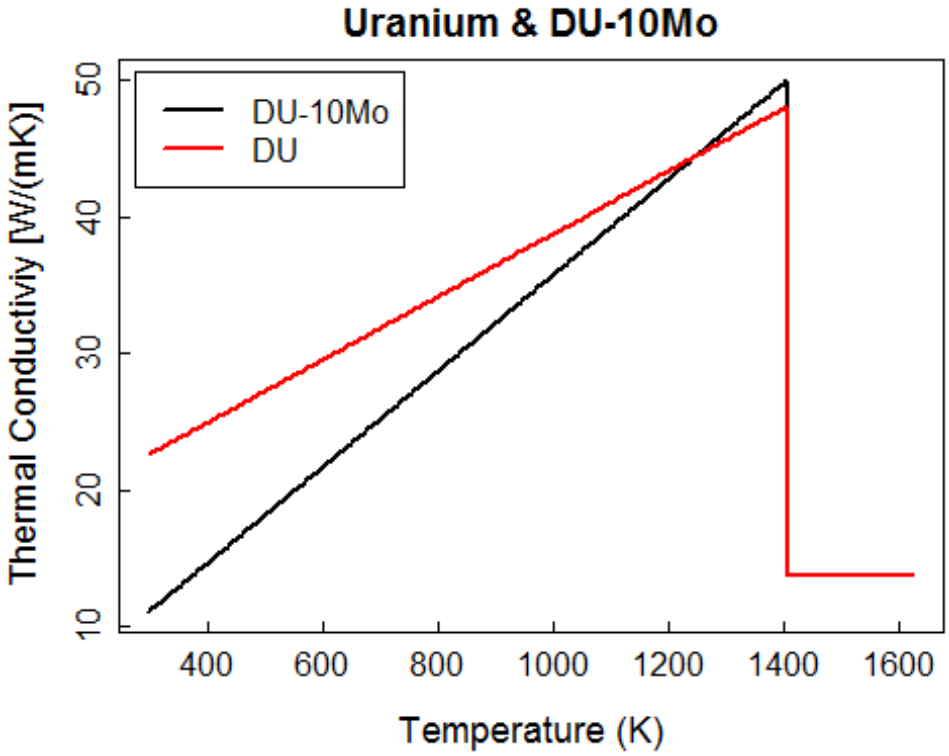

Figure 5: The thermal conductivity of pure DU and the approximate curve for DU-10Mo.

Graphite data differs from grade to grade, but for the common grades that are used for molds, this difference is most notable for the radial direction vs extruded direction conductivity. Aside from extrusion orientation, density and ash content make the biggest contributions to thermal conductivity changes. Here, as shown in Figure 6, we have used values close to the radial direction of HLM and of 2020 grade.

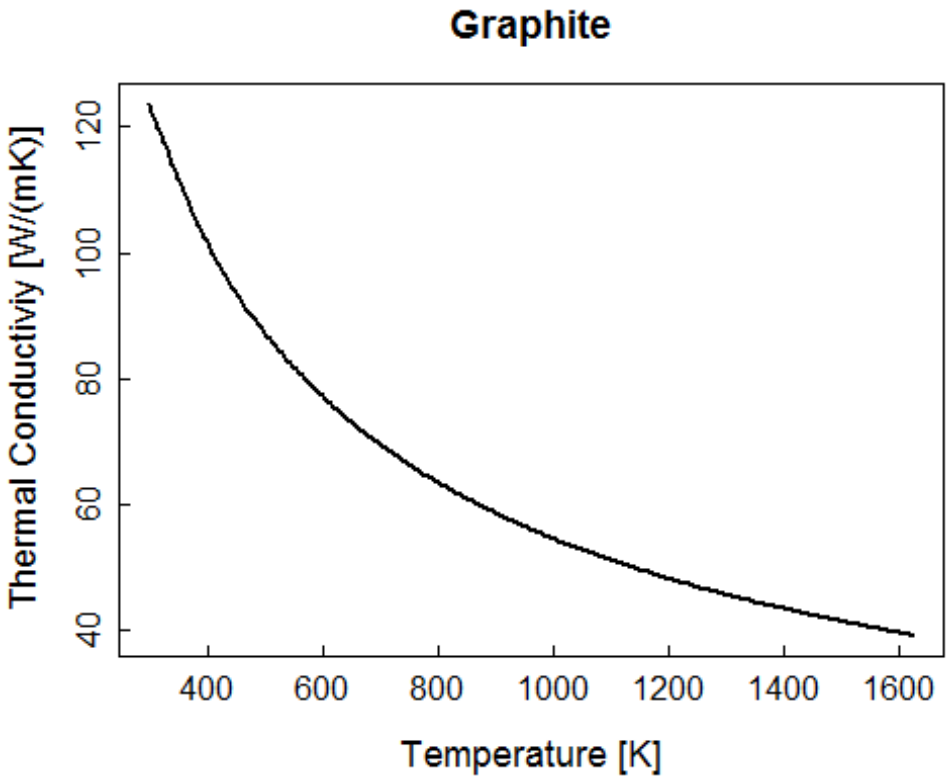

Figure 6: The thermal conductivity used for the graphite molds in this study.

3.1.4 Specific Heat

The specific heat capacity of both graphite and uranium are well known. Although the alloy is less certain, good approximations can be made with data from some sources found in reference [3]. The curves used for these experiments are not shown individually here, but instead have been combined with the density curves due to the importance of this factor to mold design.

The density and specific heat are individual components which make up a very important comparison between the metal and the mold. The product of the specific heat and the density gives us the volumetric heat capacity. One can see that for graphite and DU-10Mo, the volumetric heat capacity is quite similar. The important implications with regard to total heat balance are especially in the early stages of solidification. As the metal is first experiencing heat transfer with a mold part, the thermal boundary layer which is set up during this transient time is driven by the mass near the interface rather than a global gradient. (i.e. Growth direction will tend to be perpendicular to the mold wall rather than in the direction of the mold axis at early times)

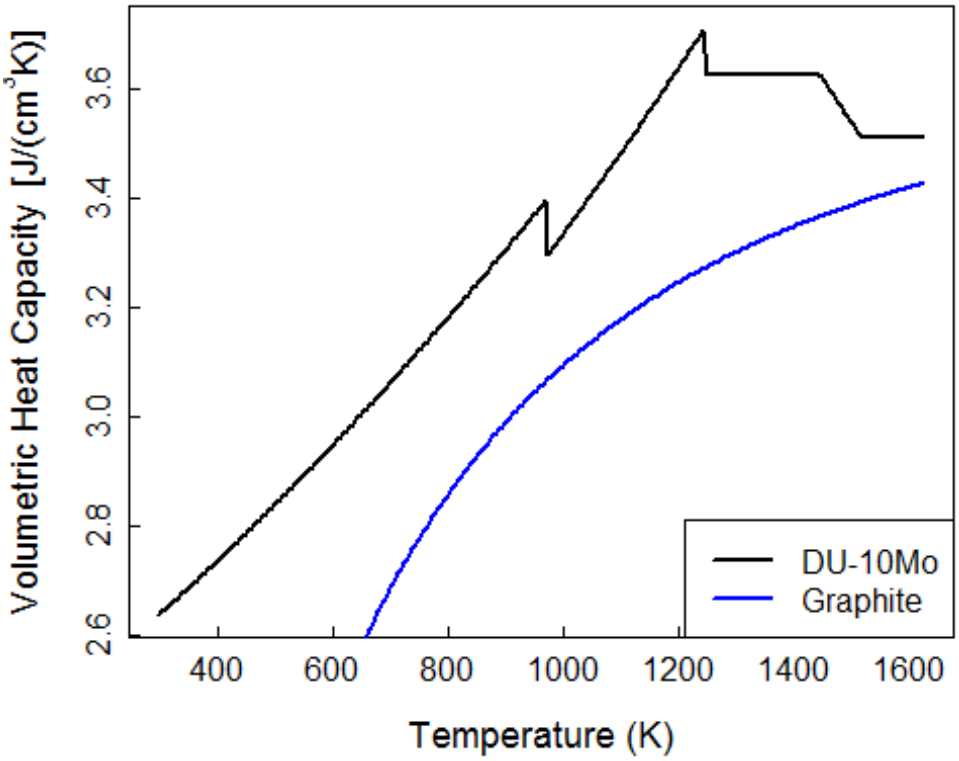

Figure 7: The volumetric heat capacity for DU-10Mo and graphite.

This effect can be assessed by examining the thermal boundary diffusion distance, *d*. A schematic representation of the thermal change across the boundary at an early time is shown in Figure 8. This diffusion length is proportional to the thermal diffusivity, α_{DT}, and time, *t*, as shown in the following equations.

$$d \approx \sqrt{4\,\alpha_{DT} t}$$

From the comparison above, at the melting point the product of density and specific heat is ~1. Therefore, substitution for the definition of the thermal diffusivity reveals that the ratio of the diffusion distances is most closely related to the ratio of thermal conductivities.

$$d \approx \sqrt{\frac{4\,kt}{\rho C_P}}$$

$$\frac{d_{Liquid}}{d_{Mold}} \approx \sqrt{\frac{k_{Liquid}}{k_{Solid}}}$$

Referring the reader back to the values for thermal conductivity near the pouring temperature, it can be seen that for 2020 graphite and for extruded grades (e.g. HLM) in the radial direction, the thermal boundary layer in the metal and in the mold are roughly same distance (which approximates to the same volume!). Therefore, it can be

shown that at short times and relatively thin mold sections, any non-axial solidification distance can be approximated as the mold wall thickness.

This revelation isn't particularly important to this monolithic geometry except for the thin sections of the irregular octagon design. More detail on this matter can be found in the design revision discussion.

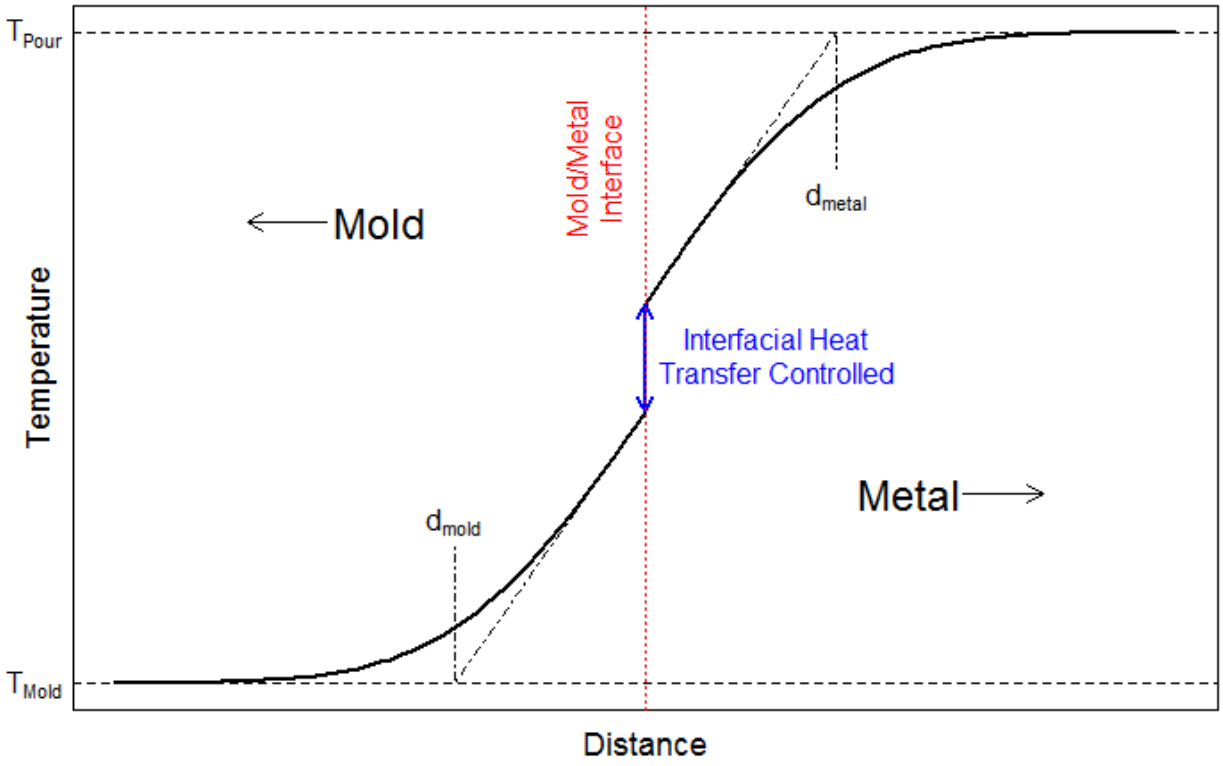

Figure 8: A schematic representation of the thermal boundary layers in the metal and mold shortly after initial contact. The interface and the approximate thermal diffusion distance are marked. The gap between the temperature curves is determined by the interfacial heat transfer coefficient.

3.2 Heat-Up Simulations

In order to determine the optimum mold stack arrangement relative to the induction coils, the software package Truchas was used to simulate mold heat-up of the casting design because of its ability to solve heating by inductive coupling. Truchas is a multi-physics, mimetic finite difference, process simulation code that has been developed at LANL to take advantage of massively parallel computing systems. The code utilizes an unstructured polygonal mesh in Exodus II format, for the current simulations the mesh file contained between 1.7 and 2.1 million unique elements. Distribution of the code onto multiple processors was performed using Message Passing Interface (MPI). The simulations presented here were run using local resources in SIGMA Division at LANL with up to 94 processors. In total, each simulation required approximately 100 processor hours to perform.

Three simulations were performed, representing three potential locations of the part mold in C-furnace at LANL. It was found that the highest location resulted in the desirable thermal gradients in the initial mold stack.

Figure 9 shows a picture of the configuration of the initial HFIR mold stack in C-furnace in the LANL foundry. During casting, metal will be placed in the crucible of the mold stack with a stopper-rod to prevent the metal from entering the mold until heating is completed. An alternating current in the induction coil (red in Figure 9) induces a current in the graphite of the mold stack, resulting in Joule heating. In order to achieve a successful casting the crucible must be heated sufficiently to melt the metal charge; however, excessive heating of the rest of the mold stack is undesirable since additional heat will result in prolonged solidification times and may result in casting defects. Ideally a thermal gradient will be imposed on the mold stack with the bottom of the mold being at least 700 °C when the crucible is hot enough to melt the metal charge.

The location of the electromagnetic coil is fixed in C-furnace, however the relative efficiency and location of heating of the graphite mold stack can be varied by changing the location of the stack within the coil. To understand the possible thermal profiles that could be generated in the initial mold configuration three mold stack positions were tested. Here we present simulations of three complete heat-up cycles, varying the position of the mold in the furnace while holding all other parameters constant.

To accurately represent the entire heat-up cycle time-resolved simulations of the entire furnace were performed on a three-dimensional mesh. Three mold configurations were represented in the simulations; the first with the mid-plane of the mold at the bottom of the coil and the other two with the mold stack shifted upward by 15 cm and 30 cm from the mid-plane position. The three simulations will be referred to as the MP, LW and HI stacks for the mid-plane, 15 cm downward shifted, and 15 cm upward shifted configurations, respectively. All other parameters for the simulations were held constant between the three mold positions and were selected based on previous casting efforts at LANL.

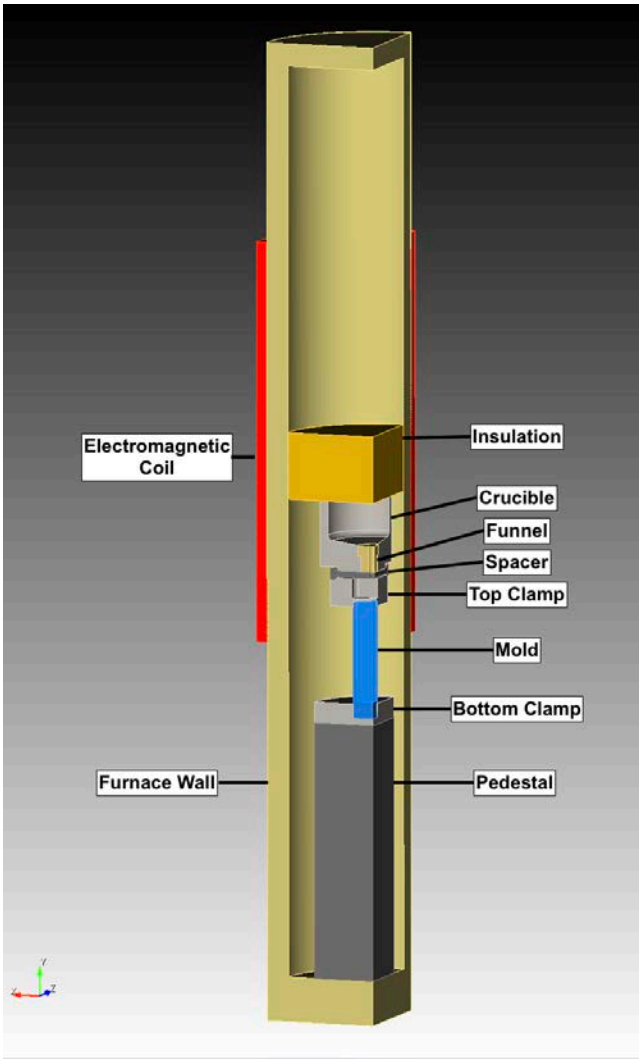

Figure 9: Picture of half the simulated domain for the HFIR mold stack in C-furnace at LANL. The position of the components labeled on the right side of the picture was varied for the three simulation conditions. The MP configuration is shown.

Figure 10 shows the relative heating of the three mold stack configurations in an equivalent electromagnetic field. The LW mold stack resulted in the maximum induced heating observed for the simulations, this heating was localized predominantly in the top region of the crucible (Figure 10b). In contrast, the HI mold stack resulted in localized heating of the outside edge of the bottom clamp and pedestal and generally uniform of the top of the mold stack. The MP mold stack resulted in diffuse heating of the top of the mold stack with minimal heating of the bottom of the mold or the pedestal.

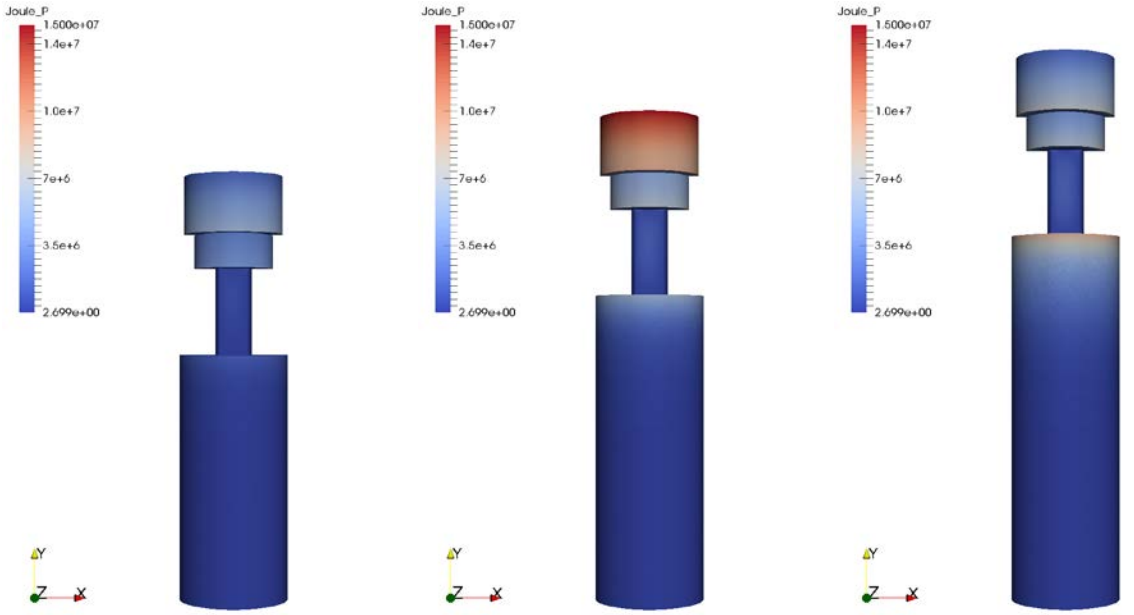

(a) (b) (c)

Figure 10: Calculated Joule power heating of the HFIR mold stack in the (a) MP, (b) LW, and (c) HI mold stack configurations. The outside surface of the mold is shown to indicate the maximum heat delivery.

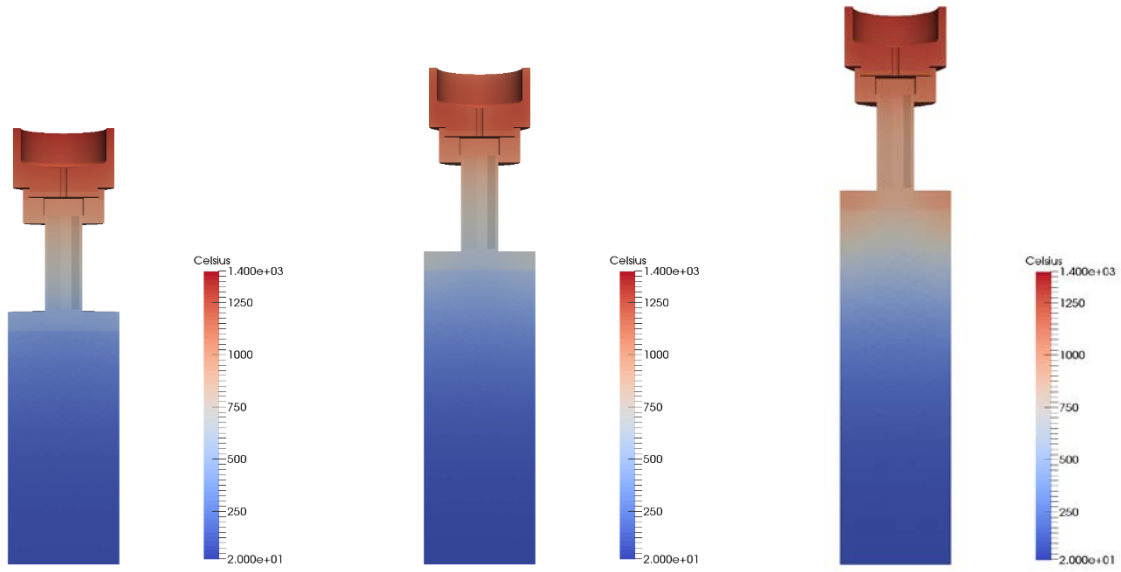

(a) (b) (c)

Figure 11: Calculated thermal profiles for the HFIR mold stack after 1800 s of heating in the (a) MP, (b) LW, and (c) HI mold stack configurations. The mid-plane surface of the mold is shown to indicate the temperatures of the surfaces where the liquid metal would interact.

Figure 11 shows the thermal profiles of the three mold stack configurations resulting from the imposed electromagnetic heating after 1800 s of heating. The three images in Figure 11 look very similar, and comparable temperatures were achieved in each simulation. All three mold stacks generated clear thermal gradients from the bottom of the mold to the crucible. However, it can clearly be seen that the HI mold configuration (Figure 11c) resulted in much higher temperatures in the bottom of the mold stack compared to the MP and LW configurations. Additionally, there was additional mold heating (compared to concentrated crucible heating) in the HI configuration, resulting in higher overall temperatures in the mold region of the HI mold stack (Figure 11c).

To quantify the trends observed in the images in Figure 11, Figure 12 shows simulated temperatures for locations where diagnostic thermocouples would be placed in each mold stack, one plot is shown for each mold stack configuration. The melt thermocouple location was placed near where the molten metal will sit prior to casting, the relatively low final temperature in the LW mold stack suggests that this configuration may have difficulty sufficiently heating the metal charge for casting. The lowest temperature in the mold with the highest concentration of heat delivery emphasizes the for complete heat-up simulations.

All three simulations indicate that a desirable vertical thermal gradient is developed across the mold with the bottom of the mold being significantly cooler than the top. The magnitude of the thermal gradient in the mold ranges from a minimum of 14 °C/cm for the HI configuration to 19 °C/cm for the MP configuration. While the lowest mold position, MP in Figure 12a, results in the greatest vertical thermal gradient from the crucible to the bottom of the mold, which would be desirable to ensure that solidification progresses from the bottom of the mold upward, there is also a pronounced lateral gradient at the bottom of the mold stack. This lateral gradient may result in the solidification progressing from the edge of the mold inward, which may result in centerline defects in the cast billet.

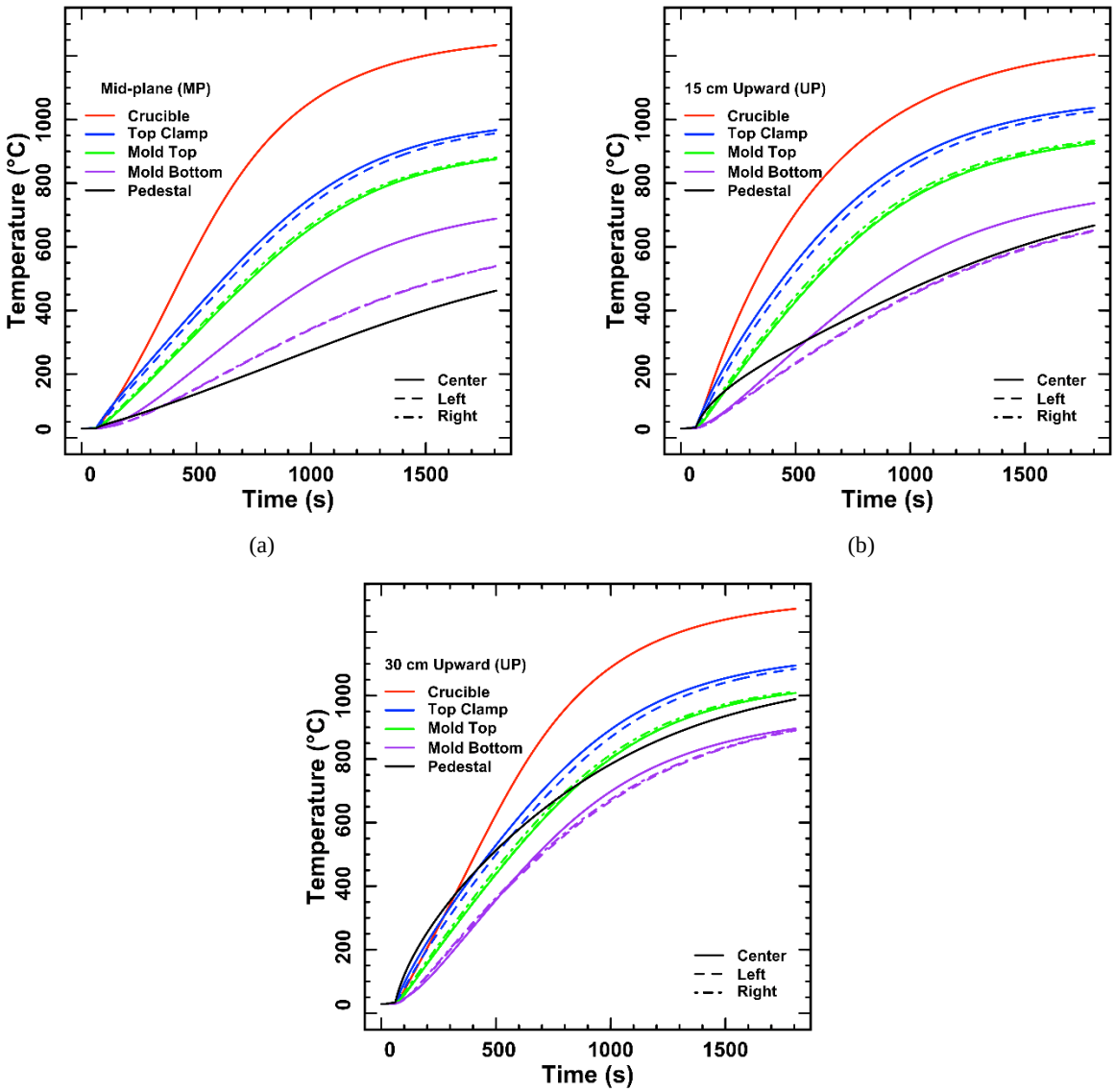

Figure 12: Temperature data from simulated thermocouple locations for the heat-cycles of the HFIR mold stack during heating in C-furnace for the (a) MP, (b) LW, and (c) HI mold stack configurations. Dashed lines are for probe locations on the mold part line (left and right side of the mold in Figure 11) while the solid lines represent probe locations along the center flat region of the mold.

4.0 Experimental trial details

Three full-scale experimental trials were planned to achieve a working understanding of the HFIR mold design. Detailed reporting of setup conditions are given in the associated documents titled “17C-808 Casting Report” and “17C-815 Casting Report”. The third casting to follow in a separate report. All other relevant information is captured in this main report.

Experimental Trails

1. *HFIR Dev 01 - 17C-808 - Version 1, trial 1*
2. *HFIR Dev 02 - 17C-815 - Version 1, trial 2*
3. *HFIR Dev 03 - XX-XXX - Version 2, trial 1*

4.1 HFIR Dev 01

This development casting is the first true test of the current mold design. The most basic level of information concerning this test casting is provided in Table 2. The casting yield was within a normal range for alloyed uranium, and the overall process yield was reasonably high. It should be noted that this casting does not address any potential isotopic mixing issues, as pre-alloyed recycled DU-10Mo was used instead of a higher alloy content master alloy with pure uranium. Although this is a high profile concept, it has been deemed to be outside the scope of this project.

Material:	DU-10Mo
Charge Mass:	11.893 kg
Casting Mass:	11.113 kg
Casting Yield:	93.4 %
Delivered Mass:	8.449 kg
Recyclable Mass:	2.621 kg
Process Yield:	71.0 %
Mold ID:	MBS-9x3.07x1.44-HFIRAA-1
Assembly ID:	ABS-9x3.07x1.44-20170511

Table 2: A summary of HFIR Dev 01 casting information (Casting ID# 17C-808).

To summarize what portions of the criteria were achieved (based upon the first part of the document): 1.) the overall length of 9 in was achieved perfectly. The slightly longer ingot length allowed for the hot top to be removed and a paper-thin skim cut on the bottom to give the final length. 2.) No cold laps were observed and the thermal gradient was acceptable from a design standpoint. The global mold gradient was ~10 K/cm at casting time. 3.) The hot top size in relation to the total cast mass (23.6 %) higher than the criteria of 15% of the total casting mass. 4.) The overall diameter of all major mold parts as well as the overall length were transferrable. 5.) Dimensional stability, as measured with conventional shop-floor tools, was excellent. Details on the casting dimensions are shown in Figure 13.

Although a superficial examination of the summary above could lead to the conclusion that the desired qualities have mostly been achieved through proper mold conception

combined with simulations, there were some features which left unknowns to be uncovered.

The first is the proportion of material left in the hot top. The goal was to achieve a sound casting using as small of a hot top as possible with a semi-arbitrary target of 15% of the total casting mass. This development run achieved a sound casting with a hot top of 23.6% of the total casting mass. While the total hot top height was less than our anticipated need, the shrinkage was slightly greater than anticipated in the length making it a higher percentage overall. This was slated to be reduced in development casting #2.

Secondly, it would have been preferable for the melt to soak at the pouring temperature for a longer period of time. Since the bottom of the mold was heating faster than expected, the decision was made to pour based upon the temperature of the bottom of the mold rather than a prescribed soak time. From a metallurgical standpoint, a hold time closer to 30 minutes would have been preferred in order to allow for sufficient out-gassing of the melt, and it would have been possible to heat the hot top region to the target temperature of 1177°C (1156°C was achieved).

Thirdly, power drift was a considerable issue during this run. At the time, the operator had assumed that this was due to an issue with the power supply. The second development casting would shed more light on this. As it happens, the decreased power (~50 kW instead of 60 kW) applied to the mold stack likely was a cause for the lack of a short soak time. The temperature of the mold base is driven largely by conduction rather than joule heating, so it allowed the mold to heat up during the longer heat-up period.

Finally, radiographic evidence (Figure 14) indicated a potential density gradient starting approximately half-way up the ingot. This is of concern because it could be evidence for macrosegregation. Although DU-10Mo has not been observed to exhibit macrosegregation due to floatation of Mo-rich dendrite fragmentation in the past, it is physically possible and occurs in other DU alloys. Alternatively, and perhaps more concerning, is that the part started to solidify from the bottom up, but instead began to solidify in near isothermal conditions in the top portion. The radiographs did not indicate any locations where there were any sizable voids. One surface feature near the bottom of the casting was confirmed to be due to a drop of extra mold coating and not due to a filling issue.

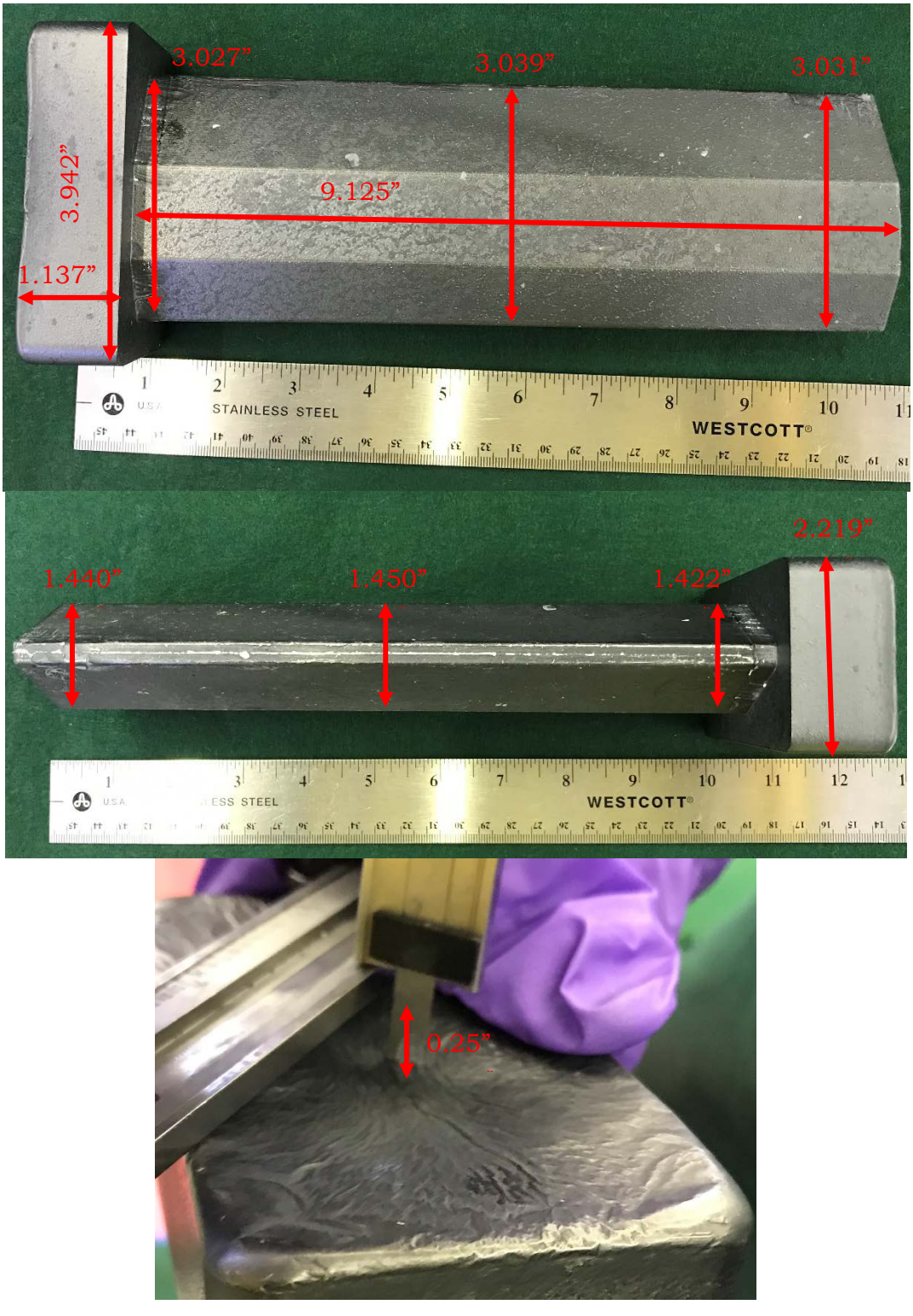

Figure 13: Final casting dimensions for 17C-808.

Figure 14: Digitized versions of radiographs of the final ingot from HFIR Dev 01 (17C-808), looking through the thick section of the ingot. The images are cropped to the exact same scale and location. The top image used a 15R source while the bottom used a 105R source. The right side of the image is the top of the ingot. The angled sides of the cross section result in these portions being nearly invisible at a high source energy. An apparent density change from the bottom of the ingot (left side) to the top (right side) is observed, with a potential saddle point in the middle.

In order to gain some information on the chemical homogeneity of the casting, several drill samples were taken from various locations in the part. Each chemical sample was split into roughly 1 g sets of chips for carbon and ICP analysis. At the base of the hot top, two samples were taken closely spaced together. These are shown in Figure 15.

The results from this chemical sampling have not been received at the time of report preparation. These results will be made available to the sponsor once they are confirmed.

After chemical sampling, the ingot was split in half length-wise. The two halves and the vertical cross section of this ingot, as shown in Figure 16, show no sign of voids or porosity. This is was an expected condition based upon the radiography data. The scratches and apparent color change in the photo were due to the machining and handling and are not representative of material-property changes. It should also be noted, that cutting speed (Electrical Discharge Machining) did not change during the cut through the material. This was noted in order to act as a qualitative data point in the discussion of macrosegregation.

General run and temperature parameters for this casting are given in Table 3. This can be directly compared to Table 3 to determine the differences between the first and second development castings. The temperature profile was quite close to the target temperatures. The power settings were adjusted several times in order to compensate for the loss of power control during the run. Additional detail concerning the mold, run parameters and thermal gradient are contained in the associated casting reports.

Figure 15: 17C-808 hot top (top) and ingot (bottom) showing the locations of chemical samples.

Figure 16: 17C-808 after sectioning. The outer surfaces are shown on the left and one of the inner surfaces is shown on the right.

Casting Plan and Summary: 17C-808				
		Date Cast:	5/12/2017	
Material:	DU-10Mo			
Mold:	Octagonal cross section Rev 1			

Furnace Details		
Parameter	Goal	Actual
Initial Power	60 kW	50-75 kW
Time at 60kW	40 min	42 min
Hold Temp	1400 °C	1400 °C
Soak Time	10-30 min	5 min

Temperatures				
Position	Goal	Actual	Deviation	TC ID
Melt	1400 °C	1397 °C	-3 °C	Pyro
Crucible	NA °C	1235 °C	NA °C	1
Hot Top	1177 °C	1156 °C	-21 °C	2
Mold Top	NA °C	1093 °C	NA °C	3
Mold Middle 1	NA °C	1052 °C	NA °C	4
Mold Middle 2	NA	NA	NA	5
Mold Bottom	900 °C	894 °C	-6 °C	6
Bottom Clamp	NA °C	897 °C	NA °C	7
Pedestal	NA °C	766 °C	NA °C	8

Table 3: Run data summary for 17C-808. Goal and actual casting parameters are listed.

4.2 HFIR Dev 02

A second development casting was performed with the first version of the mold design in order to show repeatability of the achived sound casting as well as to determine whether some irregularities were a function of the design or the individual trial. The most basic casting information is given in Table 4.

Material:	DU-10Mo
Charge Mass:	10.905 kg
Casting Mass:	10.495 kg
Casting Yield:	96.2 %
Delivered Mass:	8.546 kg
Recyclable Mass:	1.883 kg
Process Yield:	78.4 %
Mold ID:	MBS-9x3.07x1.44-HFIRAA-1
Assembly ID:	ABS-9x3.07x1.44-20170511

Table 4: A summary of HFIR Dev 02 casting information (Casting ID# 17C-815).

While not particularly important to the experiment, it should be noted that this casting started as 17C-814, but a power failure near the melting point required a restart to the casting. This "new" casting was given the next sequential number of 17C-815.

The dimensions of the final cast piece were nearly identical to 17C-808 except for the hot top height (0.84"). The final hot top mass is ~17.9% of the total casting. It should be pointed out that the yield on this casting was on the high side of the standard range. Since we planned for a consistent yield with the first development casting the hot top size is slightly higher in percent of the final casting. If the same yield had been met, this would been 15.4%. In the author's view, this meets the spirit of the 15% goal for hot top size. The total process yield is also higher due to a slightly better casting yield as well as a reduced hot top size.

During this casting run, it was imperative that the cause of the surface defect from the first development casting be identified. An extra check on mold coating condition was completed during assembly to ensure that no "dollops" were left behind as was suspected in HFIR Dev 01 / 17C-808. Indeed, no surface defects were observed in this development casting. Considering that the mold temperatures were similar between runs, it is safe to consider that the defect in the first run was not a function of the mold itself, but instead due to a distraction-driven error during assembly.

The dimensional stability of this second casting was nearly identical to the first development run (some major axis measurements were up to ~0.050 inches smaller than the designed part in the major axis. Additionally, an identical chemical sampling procedure was used for the two castings.

Casting Plan and Summary: 17C-815					
			Date Cast:	7/12/2017	
Material:	DU-10Mo				
Mold:	Octagonal cross section Rev 1				
Furnace Details					
Parameter		Goal		Actual	
Initial Power		60	kW	50-60	kW
Time at 60kW		40	min	45	min
Hold Temp		1340	°C	1345	°C
Soak Time		10-30	min	6	min
Temperatures					
Position	Goal		Actual	Deviation	TC ID
Melt	1340 °C		1345 °C	5 °C	Pyro
Crucible	NA °C		1221 °C	NA °C	1
Hot Top	1156 °C		1135 °C	-21 °C	2
Mold Top	NA °C		1072 °C	NA °C	3
Mold Middle 1	NA °C		1018 °C	NA °C	4
Mold Middle 2	NA		NA	NA	5
Mold Bottom	900 °C		902 °C	2 °C	6
Bottom Clamp	NA °C		912 °C	NA °C	7
Pedestal	NA °C		666 °C	NA °C	8

Table 5: Run data summary for 17C-815. Goal and actual casting parameters are listed.

Like its predecessor, this casting also exhibited significant power drift. In the previous casting, 17C-808 / HFIR Dev 01, the reason was unknown and was possibly attributed to the power supply. However, multiple castings were performed for other projects between Dev 01 and Dev 02, therefore, it was thought that the mold design may be contributing to this behavior. Referring back to the mold heat-up simulations and by applying SME knowledge, it was determined that a mold design change should be incorporated in order to try to mitigate this situation. While it will be discussed further in a following section, it is worth noting that the crucible-to-mold mating design could be improved to prevent abnormal coupling. Additionally, the large diameter base plate had a sharp edge around the diameter which could be a contributing factor.

4.3 HFIR Dev 03

At the time of this writing, the third development casting was not yet completed. Mold machining was delayed and schedule could not be recovered. Please see the Additional Unanticipated Tasks section for partial justification.

This casting will use master alloy plus with DU as the charge materials. The anticipated charge breakdown is shown in Table 6 below. Button production will follow Work Instruction MST-6-OP-017. All materials are traceable to recognized specifications with known pedigree. Each lot of buttons is tracked and marked appropriately. While these are not being produced for an application that requires NQA-1 levels of rigor, this work instruction specifically anticipates this need.

	Total Mass	DU Mass	Mo Mass
Total Charge	10700 g	9630 g	1070 g
Pure DU	2207.9 g	2207.9 g	0 g
DU-12.6Mo	8492.1 g	7642.9 g	1070 g

Table 6: The anticipated charge for the final confirmatory HFIR Dev 03 casting. The total charge is made up of pure DU and master alloy buttons with composition DU-12.6 wt% Mo

The third development casting, HFIR Dev 03, is planned as a confirmation of the design revisions made after the experience of the first two castings. Details concerning those revisions can be found in the following section. Similar target temperatures for mold locations should be anticipated.

5.0 Design Revision Discussion

Assessment of the thermal profile data and the resulting casting make up the main evidence for making changes to the mold design. Revised mold information is given in Figure 17 which shows gross features.

5.1 Minor changes

While the dimensional stability was quite high across the length of the part, there were two measurements which fell below the designed casting size. Therefore, the decision was made to increase the margins by 0.05”. This will provide additional machining tolerance as well as ensuring that any localized shrinkage does not fall below the design limit. The additional mass in the part is not considered to be significant compared to this consideration.

The crucible mating design in the first version was deemed to be an unnecessary complexity. The design has been modified in order to remove this complexity and to still ensure similar heat transfer compared to the first design. This modification also increases the mechanical stability of the mold assembly.

In order to continue to attain the minimalist approach to the hot top size, the charge mass has been adjusted to be consistent with the second development casting rather than the first.

Finally, part mating surfaces have tighter tolerances in order to help reduce flash.

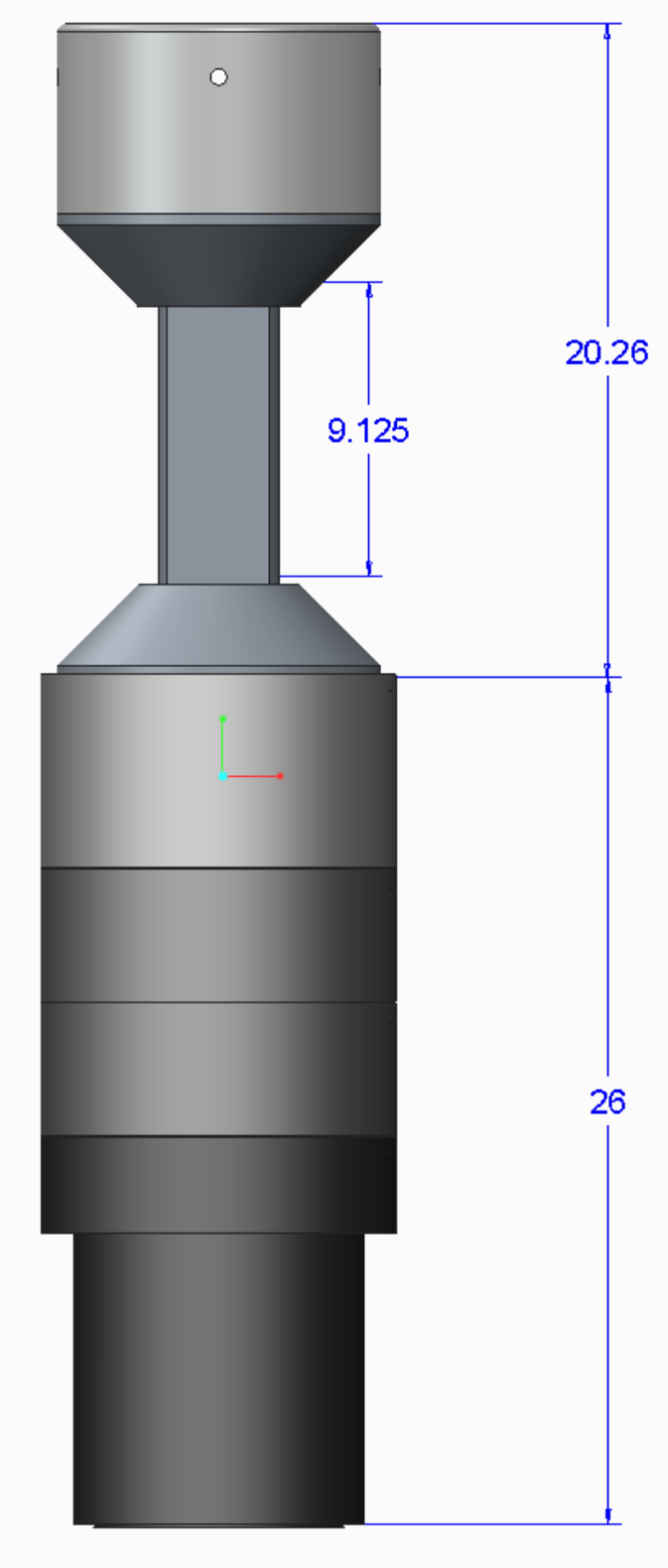

Figure 17: A front view of the revised mold stack. The overall dimension from the bottom places the mold at the appropriate height in the coils. (The bottom coil starts at 27" from the bottom). The total mold stack height remains nearly identical. The internal ingot height is shown as 9.125 inches. The remaining 0.125 inches compared to the goal height is compensation for shrinkage as well as a small machining margin.

5.2 Heat balance-driven changes

Although simulations can provide the highest detail of solidification front dynamics, it is enlightening to take a simple approach to mold/metal heat balance in order to make a design more robust to small changes. This concept can be thought of in the following way: Our simulations provide an excellent answer for an EXACT mold geometry and filling condition. Process variations could be accounted for by running large sets of process models which span the variable space, but these still only provide confidence in the light of single data points for each experiment. By taking a broader brush approach to the heat balance in the mold, we may identify mold features which could bring a region of the casting closer to an unsound design much quicker than a full parameter space matrix.

The baseline assumptions in this approach rely upon local values of the product $\rho * C_p$ as well as the temperature change necessary to induce solidification. While these terms may seem familiar from the above descriptions, they deal with a very different timescale. Instead of focusing on transient cooling of interfaces, they ignore the interfaces and rely upon total heat removed from or absorbed by the metal and mold respectively.

By splitting the mold into several sections, we can assess the local mold area compared to the local melt area (and in sectioning it this way, we also get a *dz* term in height so there is a volume association). The total difference in the mold temperature from the liquidus temperature at any localized section gives the total heat transfer necessary for solidification to start. Likewise the same procedure can be applied to the metal with the pour temperature and liquidus. These enthalpy terms are balancing with one positive and one negative. For a solidification process that proceeds from the bottom of the mold to the top, the sum of these enthalpy terms should be slightly negative (or slightly positive at the very bottom) and become more negative as it approaches the top of the casting. That being said, there is certainly a thermal-kinetic effect which can limit the effectiveness of this approach, but it provides an interesting comparison.

First the mold is divided into heights of *dz(z)*. The area of the graphite and metal, *A(z)*, is calculated at each location *z* and multiplied by *dz(z)* to get *dV(z)*. The product of density, specific heat capacity, the local volume, and the difference between the mold/melt temperature and the liquidus gives the total heat that needs to be released by the metal (or gained by the mold) for solidification to begin. For the metal there is an additional term from the heat of fusion.

These two products can then be added to determine whether or not an area will solidify based upon local mold and melt conditions. An additional point which should be made is that for a value of $\Delta H_{mold} + \Delta H_{melt} = 0$, this is the point at which additional heat transfer to a colder portion of the mold needs to take place in order to continue to freeze.

If this procedure is used with the initial mold version, a situation develops which is somewhat expected in hindsight, but is ripe for a mold design change. Figure 18 shows the mold temperature at pour time exhibited in 17C-808 and interpolated

temperatures between points. Furthermore, the sum of the melt and mold enthalpy values is shown in Figure 19. It can be seen that although over the length of the ingot itself, the values are exactly what is desired, the hot top region turns significantly positive. Although the evidence suggests that this is a significant exaggeration of the issue, it still can be addressed in the mold revision and was not seen as a major effect in the simulations. This technique can help eliminate major mold design errors, but can also make a good mold design more robust to future changes.

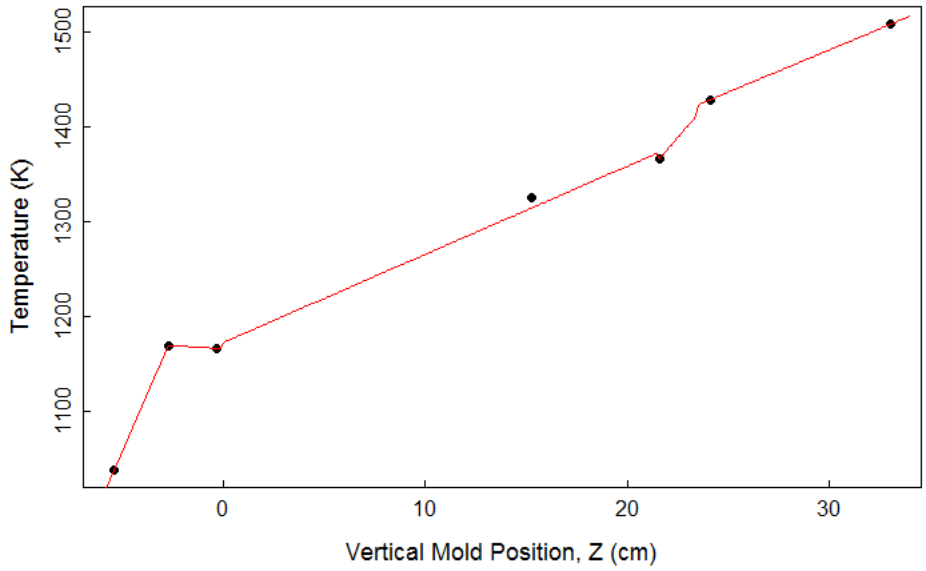

Figure 18: Mold temperatures as measured in 17C-808 (points) and the interpolated temperature values with vertical mold position. Z=0 corresponds to the bottom of the mold cavity.

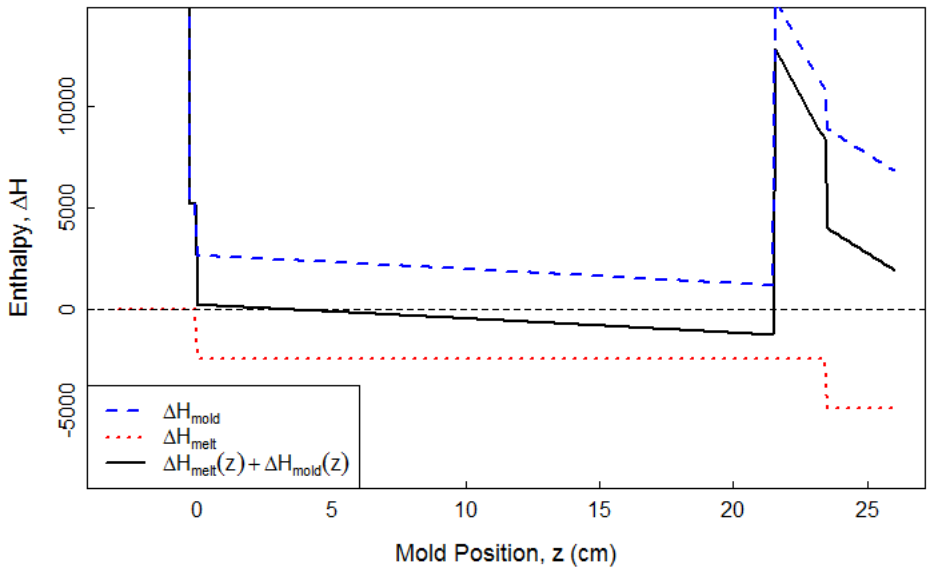

Figure 19: The local enthalpy of the melt, mold, and their sum. A negative value in this case denotes that if heat transfer were only in the plane at a single height, the liquid would have cooled but not started to solidify.

In light of this analysis, the following changes have been made in the revised design:

- The top clamp thickness has been reduced at the top of the casting.
- The bottom clamp has been changed, still retaining a similar mass.

The bottom clamp underwent the more significant visual change. In this case, the mass is important, but also the distribution of that mass. Therefore, the mass integration from the center mating point of the mold out in a spherical radius was used to attempt to match thermal properties, while also improving the design. In this case, a clamp is created which still has the same distribution of mass near the metal, but without the wide diameter so as to prevent edge coupling at the bottom of the mold. The total volume can decrease somewhat, but there should at least be more graphite in the base than total molten metal. A depiction of this process is given in Figure 20. These mold features are shown in the preceding figures.

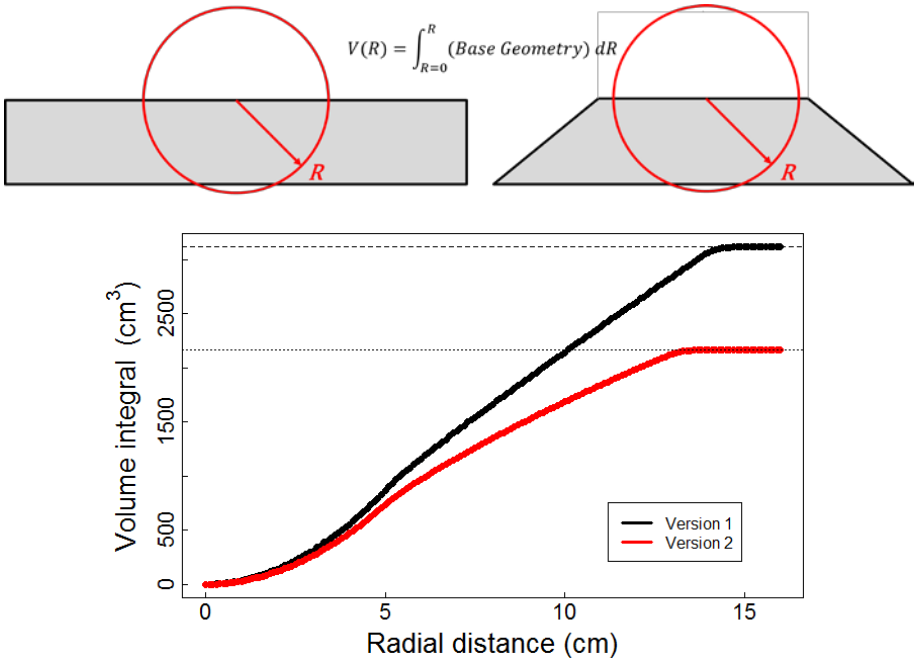

Figure 20: Schematic representations of the old and new mold geometries (top, left/right respectively) and the actual volume integral approximation showing differences between mold the versions.

6.0 Conclusion

Significant advances have been made in providing an optimized mold design for the HFIR casting. The castings produced at the time of this writing nearly meet all criteria set forth for the first step of the casting process design. While the hot top size could possibly be reduced further, it would not be recommended as a continued goal unless this design change were tested. Enough metal needs to be available for feeding and interior insulation is likely a non-starter for the final production design due to hang-up concerns. Since the initial mold design was so successful, the revised mold design minimizes any major changes. Specific engineering and use features have been added while attempting to keep the solidification conditions close to identical as possible.

A confirmatory casting is still required, but will be completed with funding provided in FY18. Information not yet available for this report at the time of submission will be provided to the sponsor.

Additional Unanticipated Tasks

Production challenges over the course of the year within the umbrella program required LANL SME travel, consultation, and data analysis, which required a considerable amount of time and effort. Partly as a result of these challenges, the program also established Integrated Product Teams (IPTs) for each manufacturing discipline. Seth Imhoff was named PI for the Casting IPT and a member of the HFIR IPT with supporting effort to be charged to this program. These time commitments have real impacts on budget and schedule since Seth Imhoff is the foundry team leader.

Acknowledgements

Beyond the authors of this report document, a considerable amount of effort was made by many individuals. Generally, the entire Sigma Foundry and Solidification Science team, but with special thanks for: Hunter Swenson, Jeff Robison, Isaac Cordova, (LANL, SIGMA). Machining support was provided by Hand Precision Machining, LLC. Additional simulation support was provided by Meghan J. Gibbs (LANL, MST-16) and John W. Gibbs (LANL, XTD-PRI). Radiography was provided by Troy K. Childers and Hideyoshi (Yoshi) Coe (LANL, AET-6). Chemical analysis was provided by Amber Telles (formerly of LANL, Sigma) and Beth Judge (LANL, C-CDE).

References

1 T. Muth, “Casting work in support of HFIR at LANL” File dated: 6/28/2016, Correspondence received: 6/28/2016
2 F.H. Ho, “Graphite design handbook”, United States: N. p., 1988. Web. doi:10.2172/714896
3 A.M. Phillips, G.S. Mickum, D.E. Burkes, “Thermophysical Properties of U-10Mo Alloy.” United States: N. p., 2010. Web. doi:10.2172/1000547.
4 INTERNATIONAL ATOMIC ENERGY AGENCY, Thermophysical Properties of Materials for Nuclear Engineering: A Tutorial and Collection of Data, IAEA, Vienna (2008).